IEEE Access
Multidisciplinary | Rapid Review | Open Access Journal

Received October 7, 2018, accepted November 1, 2018, date of publication November 9, 2018,
date of current version December 7, 2018.

Digital Object Identifier 10.1109/ACCESS.2018.2879982

Coordinated PHEV, PV, and ESS for Microgrid Frequency Regulation Using Centralized Model Predictive Control Considering Variation of PHEV Number

J. PAHASA[1] AND I. NGAMROO[2], (Senior Member, IEEE)
[1]Department of Electrical Engineering, School of Engineering, University of Phayao, Phayao 56000, Thailand
[2]Department of Electrical Engineering, Faculty of Engineering, King Mongkut's Institute of Technology Ladkrabang, Bangkok 10520, Thailand

Corresponding author: J. Pahasa (jpahasa@gmail.com)

This work was supported in part by the Office of the Higher Education Commission and in part by the Thailand Research Fund (TRF) under Grant MRG6180273.

ABSTRACT The integration of plug-in hybrid electric vehicles (PHEVs), photovoltaic (PV) generators, and energy storage systems (ESSs) into microgrids is highly anticipated. A coordinated control of PHEVs, PVs, and ESS will support frequency control in a microgrid. However, the size of the ESS depends on the surplus power of PV. The lower the surplus power is, the smaller the size of ESS. Furthermore, the number of available PHEVs vary with the cumulative number of the participating PHEVs. This variation of the number of PHEVs may reduce the PHEVs' control effect in the microgrid. This paper proposes a coordinated control of PHEVs, PVs, and ESSs for frequency control in the microgrid using a centralized model predictive control (CMPC) considering the variation of PHEV numbers. The objectives of the coordinated control are: 1) to suppress the system frequency fluctuation and 2) to minimize the surplus power of PV and, therefore, reduce the size of ESS. Simulation studies indicate that the coordinated control of PHEVs, PVs, and ESSs by the proposed CMPC is superior to that of the proportional integral derivative control and the distributed MPC in terms of minimizing the frequency fluctuation, the PV surplus power, and the ESS size.

INDEX TERMS Frequency control, photovoltaic, electric vehicle, energy storage, model predictive control, microgrid.

NOMENCLATURE

A_{pn}	Ideality factor for the $p-n$ junction.
$CMPC_{up}$, $CMPC_{mid}$, $CMPC_{low}$, $CMPC_{opt}$	Centralized model predictive control (CMPC) for upper, middle, lower, and optimal limits setting of photovoltaic (PV) inverter control signal.
E_g	Band-gap energy.
H	Control horizon of CMPC.
ISO	Solar insolation.
I_g	Generated current under the given insolation.
I_o, I_{sat}	Output and reverse saturation currents.
I_{or}	Saturation current at T_r.
I_{PV}	Current of PV module.
I_{ref}	Reference current signal from the maximum power point tracking (MPPT).
I_{rsh}	Current flow in the shunt resistance.
I_t	Short circuit current temperature coefficient.
K	Boltzmann's constant.
K_{PHEV}	PHEV gain.
P	Prediction horizon of CMPC.
P_{CONV}	DC/DC converter output power.
P_{DS}	Power of diesel generator.
P_{ESS}	Power of energy storage system (ESS).
P_{INV}	Inverter output power.
$P_{INV,LOSS}$	Inverter power loss.
P_L	Load power.
P_{PHEV}	Output power of plug-in hybrid electric vehicles (PHEV).
P_{PV}	Output power of PV.
$P_{PV,\text{module}}$	Output power of PV module.
$P_{PV,low}$, $P_{PV,up}$	Lower and upper limits of the PV power.

$P_{\max}$	Maximum PHEV power.
R_s, R_{sh}	Intrinsic series and internal shunt resistances.
T, T_r	Actual and reference temperatures.
T_{Inv}	Time constant of the PV inverter.
T_{PHEV}	PHEV time constant.
T_a, T_b	Start and finish simulation times.
T_{mod}	Temperature of PV module.
V_o	Output voltage of the PV module.
W_y, W_u	Input and control signals weighting matrices of CMPC.
d	Measured disturbance.
max	Maximum value.
n_{PHEV}	Number of PHEV.
q	Charge of an electron.
r	Reference set point of the controller.
t	Specific time.
u_{PV}	Control signal of the PV inverter.
u	Past actual control signal.
$\tilde{u}$	Future optimized control signal.
$u_{\min}$, $u_{\max}$	Minimum and maximum control signals.
y	Past actual measured output
$\tilde{y}$	Future forecasted output.
$y_{\min}$, $y_{\max}$	Minimum and maximum output feedback signals.
ΔP_{PV}, $\Delta P_{PV,ref}$	Actual and reference set point of the changes of the PV surplus power.
$\Delta\tilde{P}_{PV}$	Change of predicted output power of PV.
ΔP_{DS}	Change of output power of diesel generator.
ΔP_{Gov}	Change of governor of diesel generator.
ΔP_{Int}	Change of integrator of diesel generator.
ΔP_{PHEV}	Change of PHEV power.
$\Delta P_{PV,low}$, $\Delta P_{PV,up}$	Lower and upper limits of the PV power deviation.
$\Delta P_{PV,low,\min}$, $\Delta P_{PV,low,\max}$	Minimum and maximum lower limits of the PV power deviation.
$\Delta P_{PV,up,\min}$, $\Delta P_{PV,up,\max}$	Minimum and maximum upper limits of the PV power deviation.
Δf, Δf_{ref}	Actual and reference of the changes of frequency.
$\Delta\tilde{f}$	Change of predicted frequency.
Δn_{PHEV}	Change of PHEV number.
$\Delta\tilde{u}_{PV}$	Change of future optimized control signals of PV.
$\Delta\tilde{u}_{PHEV}$	Change of future optimized control signals of PHEV.
Δu_{PV}	Change of control signal of PV inverter.
Δu_{PHEV}	Change of control signal of PHEV.

I. INTRODUCTION

Grid-connected renewable resources increase rapidly in present power systems because of the decrease in remaining fossil fuel, the increasing energy demand, and environmental concerns, etc. [1]–[3]. Distributed generators (DGs) based on renewable energy resources, such as small hydro, wind, and photovoltaic generators (PV), are expected to be utilized as future DGs installed at the distribution level [1]. However, the output power of PV fluctuates due to weather conditions. Especially, under the high penetration of PV sources in an isolated microgrid, the intermittent PV power output causes severe frequency deviation [2], [3]. In order to smooth the fluctuations of the PV output power, an energy storage system (ESS) is usually connected to the grid at the PV location [4], [5]. The surplus power of the PV is stored in the ESS, while the smoothed PV power is supplied to the grid. Power control methods of the PV inverter with the internal ESS have been proposed to suppress frequency fluctuation [2], [3]. However, due to the investment cost of an ESS [4], [5], the size of an ESS is the first consideration when contemplating the installation of an ESS in a microgrid [4], [5].

In addition, the installation of plug-in hybrid electric vehicles (PHEVs) on the customer side has been proposed [3], [6], [7]. The bidirectional charging and discharging power control of PHEV batteries can be applied to improve the frequency control [3], [6], [7]. However, the number of controllable PHEVs depends on the cumulative number of the participating PHEVs [3], [6], [8]. As shown in [6], the variation of PHEV numbers affects the frequency control effect of the PHEVs. Therefore, the impact of the PHEV number should be considered when applying PHEVs to support frequency control.

Normally, both PVs and PHEVs are interfaced to the power grid by an inverter with the possibility to be smart nodes in the system [3]. Since the PV is able to act as a source without explicit energy limitation, the cooperation of PV and PHEV has been proposed for frequency regulation [3], [7], optimal PHEV smart charging with PV generators [9], and grid capacity enhancement [10]. In addition, technical considerations on the power conversion of PHEV and PV have been proposed in [11].

In [3], a coordinated control of the PVs, ESSs and PHEVs for frequency control using fuzzy method has been proposed. Simulation results demonstrate that the fuzzy control is able to yield an effective frequency regulation. However, the membership functions and fuzzy rules are defined based on expert knowledge and several trial-and-error experiments [3]. The fuzzy rules and membership functions need to be re-defined whenever the system parameters change. Moreover, the minimization of the PV surplus power and the ESS size has not been taken into consideration so far.

To tackle the problem of frequency fluctuation, PV surplus power, and ESS size, coordinated PHEV, PV, and ESS usage can be employed as model predictive control (MPC) [12]–[16] providing promising results, because

the MPC is able to work with multiple-input multiple-output problems [12]–[16]. Therefore, the system frequency fluctuation and the PV surplus power can be employed as the constraints to be controlled. The application of MPC for power system frequency control has been proposed in [6] and [17]–[21]. The MPC used in these works can be classified into 2 types, the centralized MPC (CMPC) [17]–[19] and the decentralized or distributed MPC (DMPC) [6], [19]–[21]. The CMPC is superior to the DMPC when the full system model can be obtained [18], [19]. Therefore, the CMPC is not only able to control all the manageable inputs within the system but is also able to improve the system wide performance [15], [18], [19]. Additionally, the CMPC has been proposed in the literatures for energy management [22], [23], power flow control [24], and outage management strategy [25].

In this paper, the CMPC is applied as coordinated control of PHEVs, PVs, and ESS in order to alleviate the system frequency fluctuation, minimize the surplus power of the PV and reduce the ESS size while considering the variation of the number of PHEVs.

In order to minimize the PV surplus power and the ESS size, a particle swarm optimization (PSO) [26] is applied in this work. The advantages of the PSO consist of a simple concept, an easy application, less need to adjust parameters, less computational time, and faster convergence speed when compared with some heuristic optimization techniques [27]–[29]. The PSO has been successfully applied for optimization of PID parameters [21], optimal sizing of a hybrid ESS [27], optimization of the MPPT algorithm for a PV system [28] and minimization of the reactive power in bidirectional DC-DC converters [29].

II. STUDY MICROGRID AND MODELING

A. MICROGRID

Figure 1 shows the microgrid system used in the study. The system consists of a 20 MW diesel generator, a 5.6 MW PV, 3.6 MW PHEVs, and 16 MW load [2], [3], [6]. The system base is 20 MW.

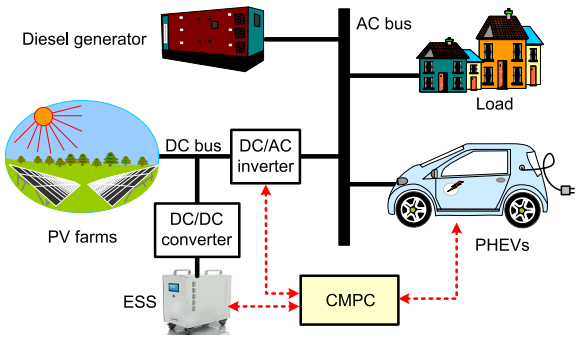

FIGURE 1. Schematic diagram of microgrid.

Generally, an energy storage is used for minimizing PV power fluctuation in Fig. 1. The surplus PV power will be fed to loads while, the power output of diesel generators is lowered. However, mismatching between generation and load causes the fluctuation of microgrid frequency. To regulate the frequency of microgrid, a droop control of diesel generator can be used. Nevertheless, since the variation of PV output power and the load change may cause severe frequency fluctuation, the diesel generator may not be able to regulate the system frequency in the acceptable range. In this work, the PV output power is fed to the microgrid so that the regulation of microgrid frequency can be achieved. In addition, the reduction of PV surplus power is used to reduce the size of battery energy storage. The PHEV energy storage is used to consume the PV power and regulate the system frequency, concurrently.

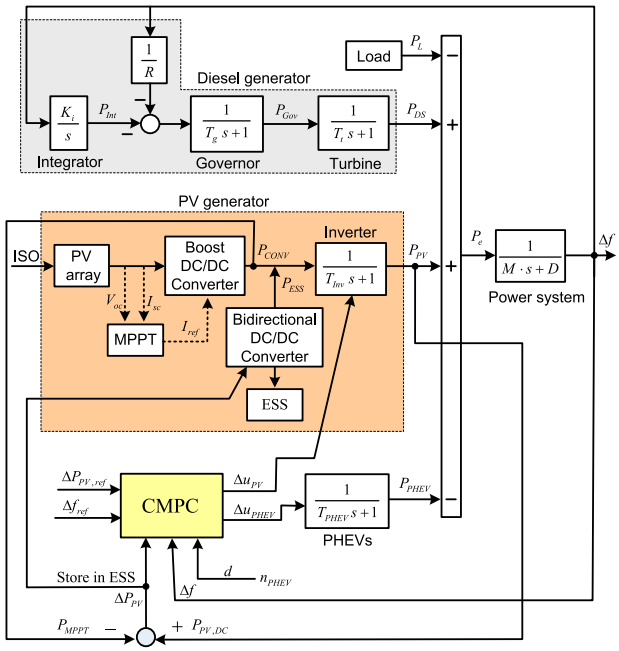

FIGURE 2. Microgrid model with the proposed CMPC.

The linearized model of the studied microgrid [2], [3], [6] is shown in Fig. 2. Here, the PV generator comprises a PV array, a boost DC/DC converter, an MPPT control, an inverter, and an energy storage system (ESS). The ESS is connected to the DC-link through a bidirectional DC/DC converter [30]. The advantage of using a DC bus for power generation and energy storage, is the reduction of the number of DC/AC inverters connected to the AC system. Rated output power of one PV module is 85 W. Therefore, 66,000 modules are used to produce 5.6 MW. Furthermore, the first-order transfer function with T_{PHEV} is used in the PHEV model [3]. Table 1 shows the system parameters [2], [6].

In this system, the CMPC is applied to calculate Δu_{PV} and Δu_{PHEV}. Additionally, n_{PHEV} is defined as the measured disturbance (d) of the CMPC.

B. PV CHARACTERISTICS

The PV module can be represented by the current source model shown in Fig. 3 [2]. The PV module parameters are

TABLE 1. System parameters.

Parameters	Value
Reference frequency, f_0 (Hz)	50
Inertia constant, M (sec)	0.2
Damping constant, D (pu)	0.12
Governor time constant, T_g (sec)	0.10
Turbine time constant, T_t (sec)	5.0
Speed regulation, R (Hz/pu MW)	2.5
Gain of integral control, K_i	0.022
Maximum number of PHEV	60,000
Time constant of PHEV, T_{PHEV} (sec)	1
PV Module	
Rated output power (W)	85
Open circuit voltage, V_{oc} (V)	22.2
Short circuit current, I_{sc} (A)	5.45
Number of cells in series, N_s	60

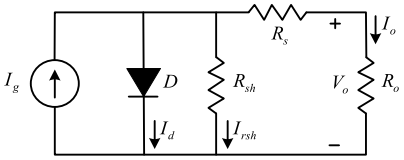

FIGURE 3. Equivalent circuit of PV module.

given in Table 1 [2]. The current in the equivalent circuit of the PV module can be expressed by

$$I_o = I_g - I_{sat}\left\{\exp\left(\frac{q}{A_{pn}KT}(V_o + I_oR_s)\right) - 1\right\}, \quad (1)$$

$$I_{sat} = I_{or}\left[\frac{T_{\text{mod}}}{T_r}\right]^3 \exp\left[\frac{qE_g}{K\,T_{\text{mod}}}\left(\frac{1}{T_r} - \frac{1}{T_{\text{mod}}}\right)\right], \quad (2)$$

$$I_g = I_{sc}\frac{S_i}{1000} + I_t\,(T_{\text{mod}} - T_r), \quad (3)$$

$$I_{rsh} = \frac{V_o}{N_sR_{sh}}. \quad (4)$$

The current-voltage $(I-V)$ and the power-voltage $(P-V)$ characteristic curves of the PV module are illustrated in Figs. 4 (a) and 4 (b).

The detailed block diagram of the current input PV module used in the study is shown in Fig. 5 [31]. This model is suitable for systems where PV modules are connected in series and share the same current. Input of the PV module consists of I_{PV} and ISO. Output consists of V_{PV} and $P_{PV,\text{module}}$. Here, I_{PV} is calculated by the MPPT algorithm.

A MPPT controller is based on the perturb and observe algorithm [2] as shown in Fig. 2. This controller which is equipped with a boost DC/DC converter, is used to track the maximum output power of the PV. Subsequently, the output power of the boost DC/DC converter is supplied to the DC/AC inverter at the maximum power point.

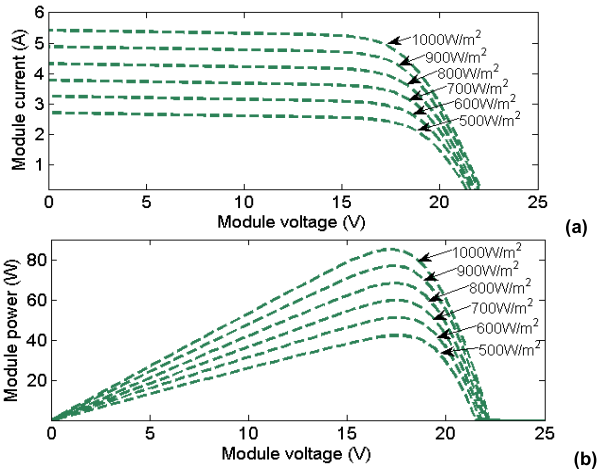

FIGURE 4. PV characteristic curves (a) $I-V$ (b) $P-V$.

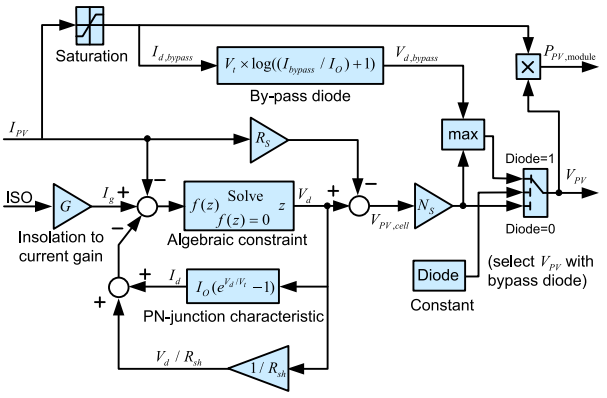

FIGURE 5. The PV module block diagram.

C. PV INVERTER AND ESS CONTROL METHODS

As shown in Fig. 2, the inverter converts the DC voltage to AC voltage. The AC power output of the inverter is then transferred to the microgrid. The relationship of P_{CONV} and P_{INV} can be expressed by (5) and (6).

$$P_{CONV} = P_{INV} + P_{INV,LOSS}, \quad (5)$$

$$P_{INV} = P_{PV} = (P_{CONV} + P_{ESS}) \cdot u_{PV}, \quad (6)$$

Here, P_{PV} can be adjusted by u_{PV} which is the output signal of the CMPC.

In addition, when the output power of the DC/DC converter is greater than the power used for frequency control, the surplus power is stored in the ESS. Conversely, when the output power of the DC/DC converter is inadequate, the power is discharged from the ESS to the microgrid. The power control of the ESS (P_{ESS}) is given by

$$P_{ESS} = \begin{cases} P_{\text{CONV}} - P_{\text{INV}}, & P_{\text{CONV}} > P_{\text{INV}}, \text{ Charge} \\ P_{\text{INV}} - P_{\text{CONV}}, & P_{\text{CONV}} < P_{\text{INV}}, \text{ Discharge} \\ 0, & P_{\text{CONV}} = P_{\text{INV}}, \text{ Neutral.} \end{cases} \quad (7)$$

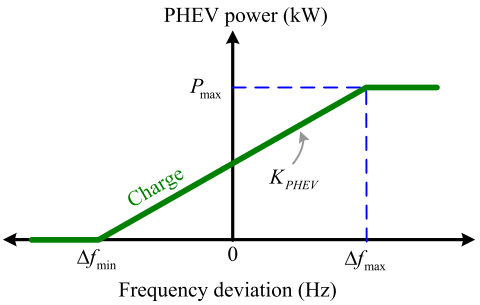

FIGURE 6. PHEV power control.

D. PHEV POWER CONTROL METHOD

In order to reduce the PV surplus power, the PHEVs consume as much power as possible within the supporting frequency control parameters. Figure 6 shows the PHEV power control. The charging power of the PHEV is controlled by the half positive droop characteristics against the frequency deviation. The active power of a PHEV (P_{PHEV}) consumed from the microgrid is designed according to the system frequency deviation (Δf) as,

$$P_{PHEV} = \begin{cases} K_{PHEV} \cdot \Delta f, & 0 < K_{PHEV} \cdot \Delta f \leq P_{\max} \\ P_{\max}, & K_{PHEV} \cdot \Delta f > P_{\max} \\ 0, & K_{PHEV} \cdot \Delta f \leq 0, \end{cases} \quad (8)$$

Here, K_{PHEV} can be adjusted by the control signal of the PHEV (u_{PHEV}) using the CMPC.

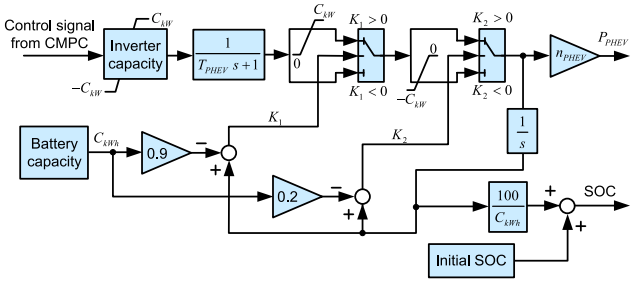

FIGURE 7. Block diagram of the PHEV module.

A detailed block diagram of a PHEV used in the study is shown in Fig. 7 [3]. The input of the PHEV model is the control signal from the CMPC. The output is the charging power of PHEV, P_{PHEV}. The inverter capacity limits the upper and lower limits of the PHEV control signal. The PHEV's battery capacity is defined based on the type of the PHEV. Besides, if the SOC of the PHEV hits the upper limit, SOC = 90%, the PHEV cannot be charged. In contrast, if the SOC of the PHEV hits the lower limit, SOC = 20%, the PHEV cannot be discharged. This SOC setting is used to prevent damages of the PHEV's battery.

III. THE PROPOSED CMPC

In this section, the CMPC for PHEV, PV, and ESS controllers are explained.

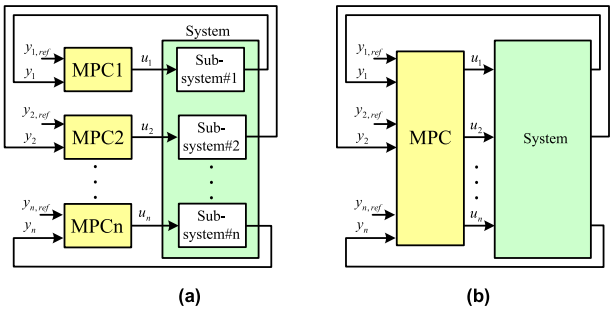

FIGURE 8. Concept of MPC (a) DMPC (b) CMPC.

A. MPC CONCEPT

The MPC concept is based on the current output signals, the linearized state-space model, and the forecasts of future values. Two types of MPC i.e., decentralized MPC (DMPC) and centralized MPC (CMPC) as shown in Fig. 8, are considered in this work.

DMPC optimizes only the local objectives and has no information about the other subsystems [15]. As shown in Fig. 8 (a), the DMPC comprises n-MPCs to compute control signals for n-subsystems. More details of the DMPC for PHEV and PV inverter control are provided in APPENDIX A.

On the other hand, a CMPC has full information to optimize overall decision variables of the full control problem [15]. As shown in Fig. 8 (b), the CMPC comprises one MPC to compute all control signals for the system. Here, the CMPC is used for the coordinated control of PHEVs, PVs and ESS, as explained in the next subsection. More details on the MPC method can be found in [12]–[16].

B. PV SURPLUS POWER SETTING CONCEPT

As shown in [32], an ESS rule-based control using forecasted reference PV output power is able to smooth PV power and reduce the ESS size. A changing reference set point of the PV power is able to reduce charge/discharge cycles of the ESS. However, the prediction of reference PV output power especially on a cloudy day may not achieve the prediction results precisely. Imprecise reference PV output power may cause the PV surplus power higher than expected.

Therefore, the concept of feasible PV surplus power variation ranges as shown in Fig. 9 has been proposed in this work. The PV inverter control signal is able to vary between $P_{PV,\,low}$ and $P_{PV,\,up}$. Various settings of $P_{PV,\,low}$ and $P_{PV,\,up}$ cause different cumulative surplus power to the ESS.

Figure 9 (a) shows the PV surplus power setting to produce a constant SOC level. After the ESS participating in the system, the SOC level may not increase or decrease. Figure 9 (b) shows the PV surplus power setting to decrease the SOC of the ESS. After the ESS participating in the system, the SOC level may be lower than before participating. On the other hand, Fig. 9 (c) shows the PV surplus power setting to increase the SOC of the ESS. After the ESS participating

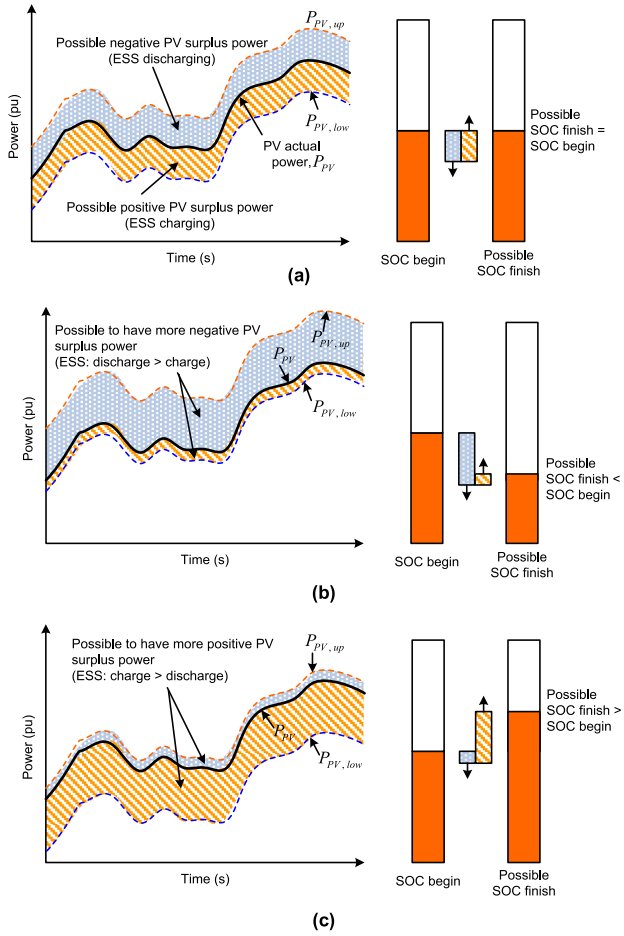

FIGURE 9. Concept of PV surplus power setting and the level of SOC of ESS when the PV and ESS participated in LFC based CMPC (a) produce equal SOC (b) to decrease SOC (d) to increase SOC.

in the system, the SOC level may be higher than before participating.

C. CMPC FOR PHEV, PV INVERTER AND ESS CONTROL

Figure 10 shows the concept of the CMPC method [13], [17] for the coordinated control of PHEVs, PVs, and ESS. For the PV power control method (see Fig. 9) the upper and lower limits of the PV power at the inverter ($P_{PV,up}$, $P_{PV,low}$) are defined and used in the CMPC. The CMPC calculates the PV inverter control signal to produce PV power varied among $P_{PV,up}$ and $P_{PV,low}$. Here, P_{PV}, $P_{PV,low}$, and $P_{PV,up}$ in Fig. 9 have been converted to ΔP_{PV}, $\Delta P_{PV,low}$, and $\Delta P_{PV,up}$ in Fig. 10 by

$$\left.\begin{aligned}\Delta P_{PV} &= P_{PV} - P_{MPPT}\\ \Delta P_{PV,low} &= P_{PV,low} - P_{MPPT}\\ \Delta P_{PV,up} &= P_{PV,up} - P_{MPPT}\end{aligned}\right\} \tag{9}$$

As mentioned earlier, the design of the CMPC has two objectives, firstly, to reduce the microgrid frequency fluctuation, secondly, the reduce the surplus power of the PV. Therefore, the input variables of the CMPC are $y = [\Delta f,\ \Delta P_{PV}]$ and the reference set point of the controller,

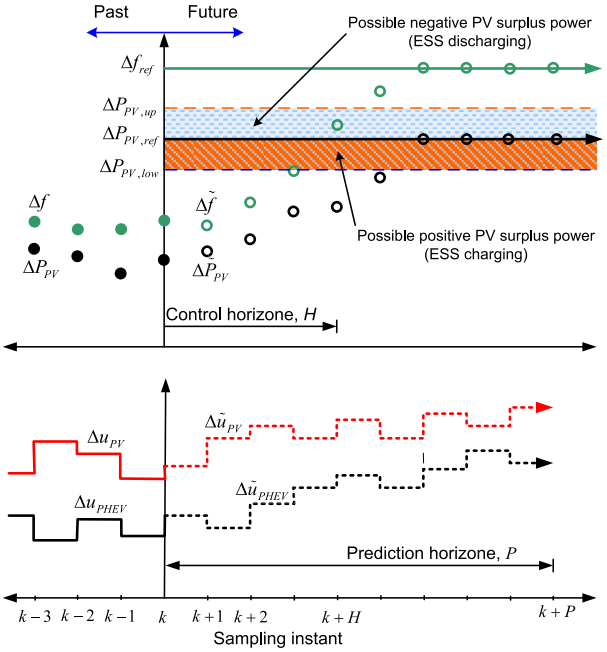

FIGURE 10. Concept of CMPC for the coordinated control of PHEV, PV and ESS.

$r = [\Delta f_{ref},\ \Delta P_{PV,ref}]$, (see Figs. 2 and 10). Additionally, the outputs of the CMPC are used as control signals, i.e., $u = [\Delta u_{PV},\ \Delta u_{PHEV}]$.

The discrete-time linear systems with state space representation of the microgrid in Fig. 2, can be defined as,

$$x(k+1) = A \cdot x(k) + B \cdot u(k) + G \cdot d(k), \tag{10}$$
$$y(k) = C \cdot x(k) + E \cdot u(k),$$

$$A = \begin{bmatrix} \frac{-1}{T_{Inv}} & 0 & 0 & 0 & 0 & 0 \\ 0 & \frac{-1}{T_t} & 0 & \frac{1}{T_t} & 0 & 0 \\ 0 & 0 & 0 & 0 & K_i & 0 \\ 0 & 0 & \frac{1}{T_g} & \frac{-1}{T_g} & \frac{1}{RT_g} & 0 \\ \frac{1}{M} & \frac{1}{M} & 0 & 0 & \frac{-D}{M} & \frac{1}{M} \\ 0 & 0 & 0 & 0 & 0 & \frac{-1}{T_{PHEV}} \end{bmatrix},$$

$$B = \begin{bmatrix} 1 & 0 \\ 0 & 0 \\ 0 & 0 \\ 0 & 0 \\ 0 & 0 \\ 0 & 1 \end{bmatrix},\quad C = \begin{bmatrix} 0 & 0 & 0 & 0 & 1 & 0 \\ -1 & 0 & 0 & 0 & 0 & 0 \end{bmatrix},$$

$$E = \begin{bmatrix} 0 & 0 \\ 0 & 0 \end{bmatrix},\quad G = \begin{bmatrix} 0 & 0 & 0 & 0 & 1 & 0 \end{bmatrix}^T,$$
$$x = [\Delta P_{PV}\ \Delta P_{DS}\ \Delta P_{Gov}\ \Delta P_{Int}\ \Delta f\ \Delta P_{PHEV}],$$
$$u = \begin{bmatrix} \Delta u_{PV} & \Delta u_{PHEV} \end{bmatrix},\quad d = [\Delta n_{PHEV}],$$
$$y = \begin{bmatrix} \Delta f & \Delta P_{PV} \end{bmatrix}, \tag{11}$$

The objective of the MPC is to compute an optimal set of control signals using the optimization problem as,

$$\min_{u(k)\in H} \left\{ \sum_{j=1}^{H} [y(k+j) - r(k+j)]^T W_y [y(k+j) - r(k+j)] + [u(k) - u(k-1)]^T W_u [u(k) - u(k-1)] \right\},$$
$$\text{subject to } y_{\min} \le y \le y_{\max}, \quad u_{\min} \le u \le \Delta u_{\max}. \quad (12)$$

The optimal output of the microgrid should be located close to the set point of the control action, i.e., $[\Delta f_{ref},\ \Delta P_{PV,ref}]$. Consequently, the first predicted control signals, i.e., $[\Delta\tilde{u}_{PV}(k+1),\ \Delta\tilde{u}_{PHEV}(k+1)]$ are employed as the actual input control signals for the PVs and PHEVs.

D. OPTIMIZATION OF THE ESS SIZE

As shown in Fig. 2, the PV surplus power, ΔP_{PV}, is stored in the ESS. The state of charge (SOC) of the ESS shows the cumulative surplus power of the PVs. As proposed in [27], [33], and [34], the SOC variation of the ESS is able to represent the size of the ESS.

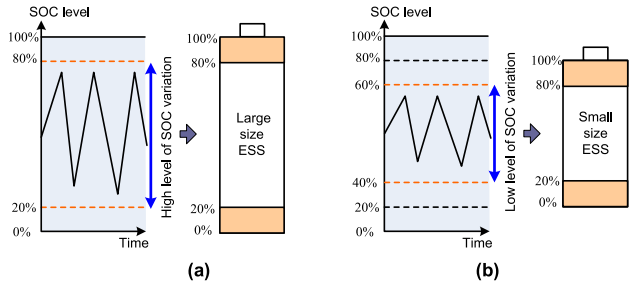

FIGURE 11. SOC variation and ESS size (a) high level of SOC variation consistent to large size ESS (b) low level of SOC variation consistent to small size ESS.

The variation of the SOC level and the ESS size can be displayed as shown in Fig. 11(SOC patterns are applied from [29]). When the magnitude of the SOC variation is high, the size of the ESS is large as shown in Fig. 11(a). In contrast, when the magnitude of the SOC variation is low, the size of the ESS is small as shown in Fig. 11 (b). Therefore, a minimization of the SOC variation is able to minimize the size of the ESS. Here, the SOC of the ESS is set to operate in the range of 20% - 80% to increase the lifetime of the ESS [27], [33] and to avoid potential damage to the ESS [34].

Furthermore, as shown in Figs. 9 and 10, ΔP_{PV} can be minimized by tuning the upper and the lower limits of the PV power deviation ($\Delta P_{PV,up}$ and $\Delta P_{PV,low}$). Here, the $\Delta P_{PV,up}$ and $\Delta P_{PV,low}$ are simultaneously optimized by the PSO [26]. The objective function based on the SOC deviation of the ESS (ΔSOC_{ESS}) can be expressed by

$$\text{Minimize } \Delta\text{SOC}_{ESS} = \max \left| SOC_{ESS,T_a} - SOC_{ESS}(t) \right|_{t=T_a}^{t=T_b},$$
$$\text{Subject to } \Delta P_{PV,low,\min} \le \Delta P_{PV,low} \le \Delta P_{PV,low,\max},$$
$$\Delta P_{PV,up,\min} \le \Delta P_{PV,up} \le \Delta P_{PV,up,\max}, \quad (13)$$

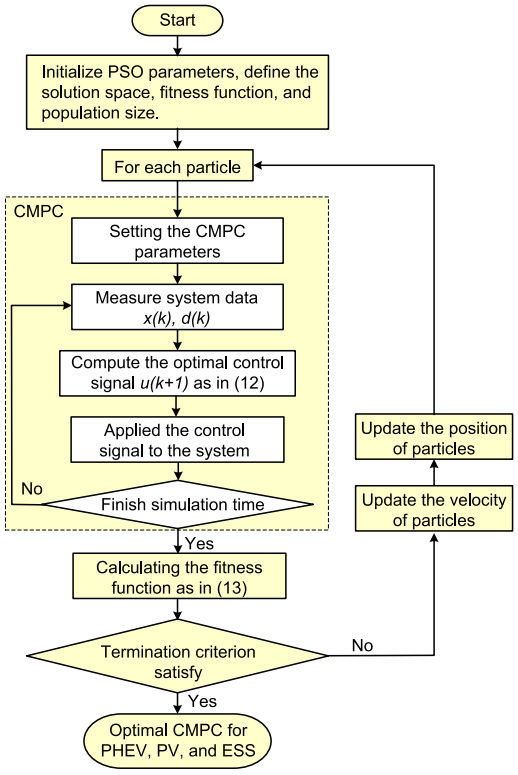

FIGURE 12. Flowchart of PSO based CMPC parameters optimization.

Figure 12 shows a flowchart of a PSO based CMPC parameter optimization used in this work.

IV. SIMULATION RESULTS

The effectiveness of the proposed method is evaluated in the microgrid shown in Fig. 2 by MATLAB/Simulink. In this work, the CMPC is applied to the coordinated control of PHEVs, PVs, and ESS to reduce the microgrid frequency deviation and the surplus power of the PV generator.

In the control design, the CMPC parameters are defined as follows: sampling time interval = 0.1 s, P = 10 samples, H = 3 samples, Δf_{ref} = 0.00 Hz, and $\Delta P_{PV,ref}$ = 0.00 pu. Besides, for the optimization of the CMPC, the PSO is defined as follows: population size = 24, minimum weighting functions = 0.4, maximum weighting functions = 0.9, the local and global best positions relative weights = 2, maximum particle velocity = 4, and maximum iteration = 150.

In the simulation study, it is supposed that the random solar insolation (ISO), PHEV number variations, and random load deviation as shown in Fig. 13 are applied to the study microgrid. Here, the PHEV number variations are assumed based on the method in [7] with a time slot of 10 s. The ISO is generated randomly based on the actual data in [3]. Additionally, the load model in [6] is employed. More details of the case studies are given here:

Case 1: The investigation of the CMPC output constraints of the ΔP_{PV} is provided. Table 2 shows the ranges of CMPC

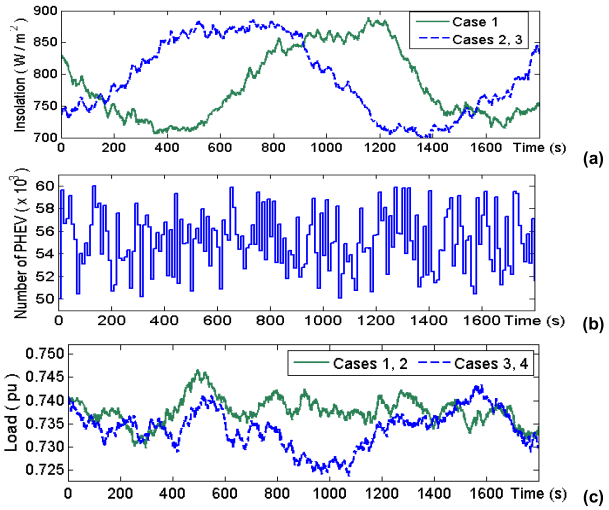

FIGURE 13. Case study (a) solar insolation (b) number of PHEV (c) random load.

TABLE 2. Ranges of CMPC parameters setting (pu) for Case I.

Model	CMPC constraints		Output constraints		ΔSOC_{ESS}
	Δu_{PV}	Δu_{PHEV}	$\Delta f(\times 10^{-4})$	ΔP_{PV}	
$CMPC_{up}$	[0.16 0.23]	[0.0 0.002]	[−2 2]	[−0.1 0.0]	41.354
$CMPC_{mid}$	[0.16 0.23]	[0.0 0.002]	[−2 2]	[−0.1 0.1]	9.295
$CMPC_{low}$	[0.16 0.23]	[0.0 0.002]	[−2 2]	[0.0 0.1]	18.820
$CMPC_{opt}$	[0.16 0.23]	[0.0 0.002]	[−2 2]	[−0.008 0.174]	5.771

parameters setting for $CMPC_{up}$, $CMPC_{mid}$, $CMPC_{low}$ and $CMPC_{opt}$. Here, the $CMPC_{opt}$ is optimized using the PSO objective function as in (14). Therefore, the optimal lower and upper limits of the PV power deviation obtained are, $[\Delta P_{PV,low}\ \Delta P_{PV,up}] = [-0.008\ \ 0.174]$. It can be seen that the ranges of ΔP_{PV} in Table 2 are set to produce upper, middle, lower, and optimal limits of the PV control signals.

The simulation results of case 1 are shown in Fig. 14. The system frequency deviation is displayed in Fig. 14 (f). It can be seen that the $CMPC_{up}$, $CMPC_{mid}$, $CMPC_{low}$, and $CMPC_{opt}$ are able to reduce the deviation of frequency. The output power of PVs and PHEVs are shown in Figs. 14 (a) and 14 (b). It can be observed that the PV inverters produce power to reduce system frequency deviation when the charging power of PHEVs hits the lower or upper limits. Besides, when the PV generators are operated under the MPPT, the PHEVs consume power to reduce system frequency variation. However, the PV generators controlled by the CMPC are able to control some gaps, e. g. the variation of the PV power from the MPPT power, as shown in Fig 14. Therefore, the setting of different ranges of minimum and maximum signals leads to different surplus power of the PV generators.

The SOC of PHEVs is shown in Fig. 14 (c). It can be distinguished that the $CMPC_{low}$ is able to yield a higher SOC in comparison with other methods. In contrast, the SOC of the $CMPC_{up}$ is lower than that of the others.

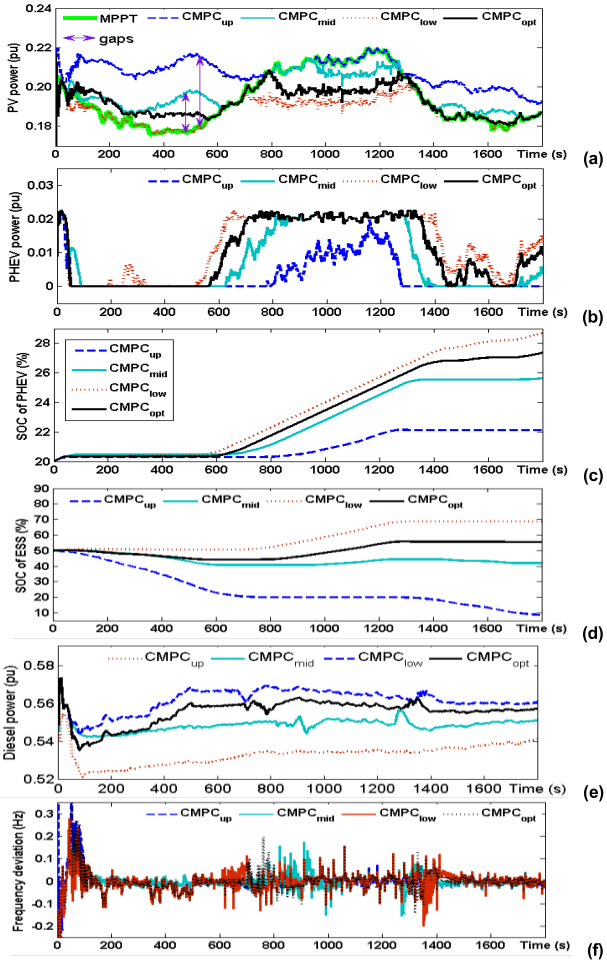

FIGURE 14. Case 1: simulation results (a) PV power (b) PHEV power (c) SOC of PHEV (d) SOC of ESS (e) diesel power (f) frequency deviation.

Figure 14 (d) shows the SOC of the ESS. At the beginning of the simulation time, the SOC of the ESS is set at 50%. At the end of the simulation time, i.e., $t = 1800$ s, the SOC using the parameters of $CMPC_{up}$, $CMPC_{mid}$, $CMPC_{low}$, and $CMPC_{opt}$ are about 9%, 41%, 69%, and 56%. These results imply that the ESS's energy capacity under $CMPC_{up}$, $CMPC_{mid}$ and $CMPC_{low}$ situations needs to be larger than under a $CMPC_{opt}$ situation. When employing $CMPC_{up}$ settings the initial power is stored in the ESS to support the system. In contrast, the PVs surplus power is stored in the ESS of $CMPC_{low}$. The ESS needs a smaller capacity under $CMPC_{opt}$ conditions when compared with the other two cases. Therefore, the $CMPC_{opt}$ is employed in cases 2-4.

Case 2: The CMPC is compared to conventional methods, i.e., the PVs and PHEVs controllers based on the proportional integral derivative (PID), and the PVs and PHEVs controllers based on the distributed MPC (DMPC). Figure 15 displays the simulation results of case 2. The deviation of the frequency when using CMPC is lower when compared to the PID or the DMPC method. Moreover, the SOC of the PHEV battery produced by the CMPC is higher than that of the

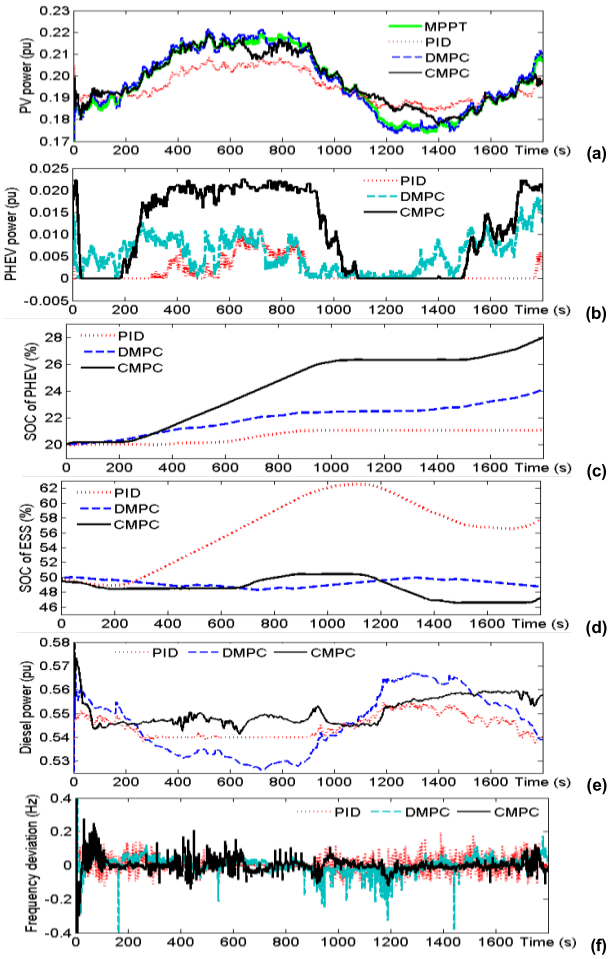

FIGURE 15. Case 2: simulation results (a) PV power (b) PHEV power (c) SOC of PHEV (d) SOC of ESS (e) diesel power (f) frequency deviation.

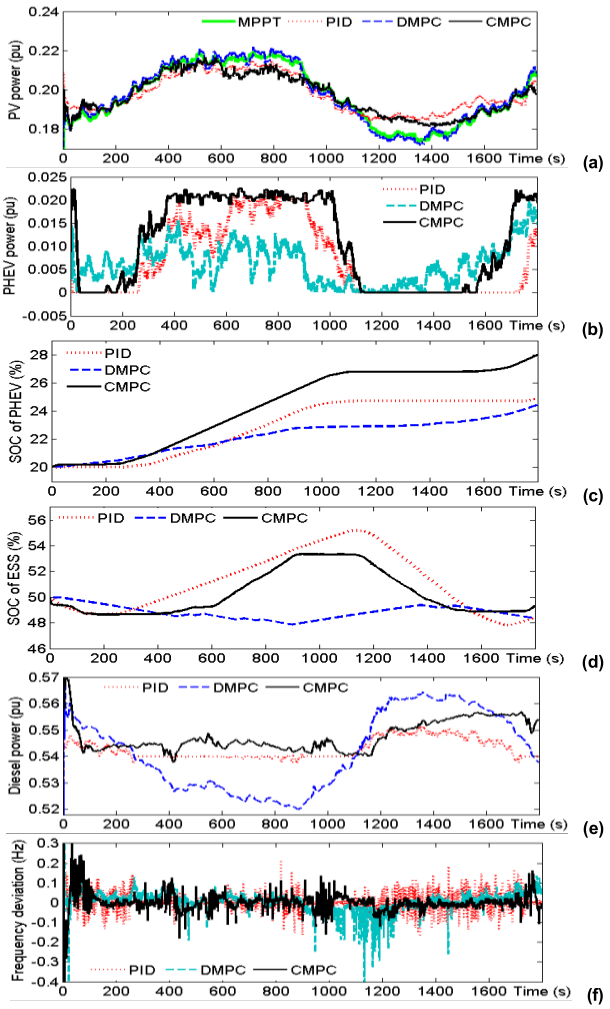

FIGURE 16. Case 3: simulation results (a) PV power (b) PHEV power (c) SOC of PHEV (d) SOC of ESS (e) diesel power (f) frequency deviation.

PID and the DMPC. In addition, the SOC of the ESS generated by the CMPC and the DMPC is lower than that of the PID.

Case 3: The proposed CMPC is compared to the PID and the DMPC against ISO patterns, PHEV numbers, and a random load as shown in Fig. 13. Figure 16 shows the simulation results of case 3. The simulation results verify that the CMPC provides a better control effect on the frequency deviation and SOC production than the PID and the DMPC.

Case 4: The CMPC effect against the severe variation of thePHEV number is evaluated. In this case, it is assumed that around 11:30 - 12:30 h, some PHEV owners plug-out their PHEVs and leave for lunch break. Subsequently, around 12:30-13:30 h, some PHEV owners return to plug-in their PHEVs. The number of the PHEVs and the solar insolation from 11:30 to 13:30 h are shown in Fig. 17. Note that the time slot for the PHEV numbers is 5 minutes according to the time slot of integrating PHEVs at the charging stations [35].

Figure 18 exhibits the simulation results of case 4. Figure 18 (f) displays the system frequency deviation.

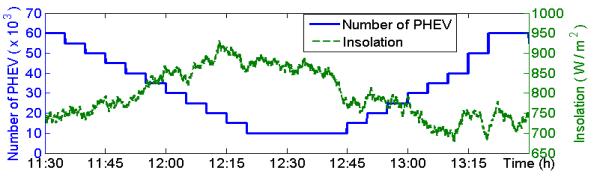

FIGURE 17. PHEV number and insolation of case 4.

The frequency deviation of the CMPC is lower than that of the PID and the DMPC. Figures 18 (a) and 18 (b) show the PV power and the PHEV power. When the PHEV power hits the minimum or maximum limits, the PV produces power to suppress the frequency deviation. Simulation results approve that the CMPC is robust against the uncertainty of the PHEV numbers compared to the PID and the DMPC.

Table 3 shows a comparison of the frequency deviation, the PV surplus power, and the maximum SOC of the ESS of the 3 methods. The CMPC is able to reduce frequency deviation better than the PID and DMPC, for all 3 cases. The PV surplus power of CMPC is very low when compared to the PID and DMPC methods. For the ESS, the CMPC is able

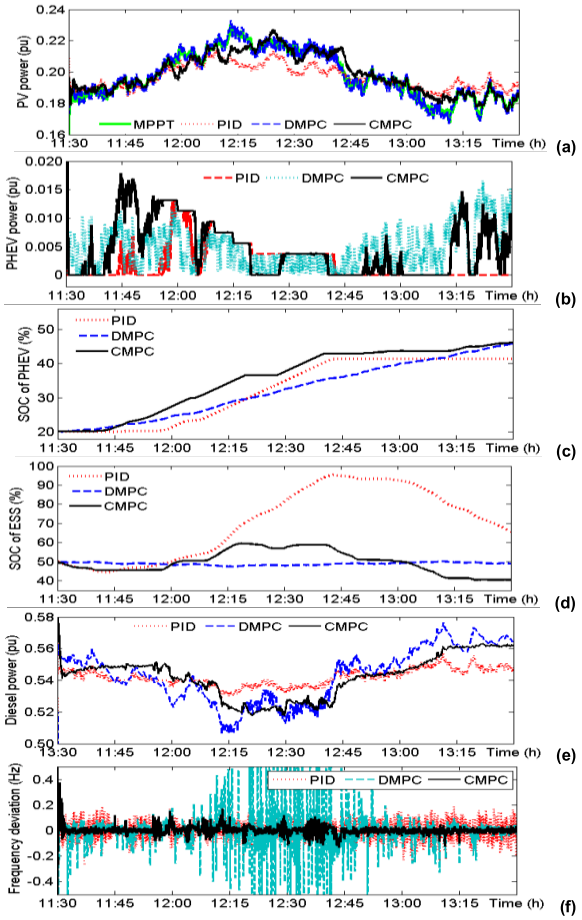

FIGURE 18. Case 4: simulation results (a) PV power (b) PHEV power (c) SOC of PHEV (d) SOC of ESS (e) diesel power (f) frequency deviation.

TABLE 3. Comparison of simulation results of the 3 methods.

Case	Maximum Δf			PV surplus power			Maximum SOC of ESS		
	PID	DMPC	CPMPC	PID	DMPC	CPMPC	PID	DMPC	CPMPC
2	1.56	7.83	1.34	4.50	-0.74	-3.54	62.54	50.03	49.56
3	1.68	7.98	1.36	-0.94	-0.97	-0.14	55.18	50.00	53.35
4	1.79	7.58	1.17	9.21	-0.63	-5.31	95.29	50.19	59.52

to produce lower ESS size than the PID. Clearly, the CMPC is better than DMPC and PID when considering the frequency deviation, PV surplus power, and ESS size.

V. CONCLUSION

The coordinated control of PHEVs, PVs, and ESS for microgrid frequency control using the proposed CMPC considering the variation of PHEV numbers has been presented in this paper. The study results can be concluded as follows:

(1) The CMPC is not only able to reduce the system frequency deviation, but also minimize the surplus power of the PVs and the size of the ESS.

(2) In case of the CMPC, when the charging power of PHEVs hits the lower or upper limits, the PV produces the power necessary to reduce the system frequency deviation. Furthermore, when the PV operates under the MPPT, the PHEVs consume the power to suppress the system frequency fluctuation. Moreover, under the uncertainty of the plug-in and plug-out of PHEVs, the CMPC is able to reduce system frequency deviations successfully against the variation of the PHEV number.

(3) The CMPC yields superior control effects when compared to the PID and the DMPC in terms of the suppression of frequency deviation, the reduction of the PV surplus power, and the minimization of the ESS size.

APPENDIX

A. DMPC FOR PHEV AND PV INVERTER CONTROL

In this work, the DMPC as shown in Fig. 8 (a) with $n = 2$ is applied to control the PHEVs and the PV inverter. Therefore, MPC1 and MPC2 are used for the PHEV and the PV inverter controllers, respectively. More details are as follows:

MPC1: The state space of the control loop and the MPC calculation for PHEVs can be expressed in (14)-(17).

$$\begin{bmatrix} \Delta \dot{P}_{PHEV} \\ \Delta \dot{f} \end{bmatrix} = \begin{bmatrix} \frac{-1}{T_{PHEV}} & 0 \\ \frac{-1}{M} & \frac{-D}{M} \end{bmatrix} \begin{bmatrix} \Delta P_{PHEV} \\ \Delta f \end{bmatrix} + \begin{bmatrix} \frac{1}{T_{PHEV}} \\ 0 \end{bmatrix} \Delta u_{PHEV} \tag{14}$$

$$[\Delta y] = \begin{bmatrix} 0 & 1 \end{bmatrix} \begin{bmatrix} \Delta P_{PHEV} \\ \Delta f \end{bmatrix} + [0]\, \Delta U_{PHEV}, \tag{15}$$

$$x(k+1) = A_{PHEV} \cdot x(k) + B_{PHEV} \cdot u(k) + G_{PHEV} \cdot d(k) \tag{16}$$

$$y(k) = C_{PHEV} \cdot x(k) + E_{PHEV} \cdot u(k) \tag{17}$$

where

$$A_{PHEV} = \begin{bmatrix} -1/T_{PHEV} & 0 \\ -1/M & -D/M \end{bmatrix}, \; B_{PHEV} = \begin{bmatrix} 1/T_{PHEV} \\ 0 \end{bmatrix},$$
$$C_{PHEV} = \begin{bmatrix} 0 & 1 \end{bmatrix}, \quad E_{PHEV} = [0], \text{ and } G_{PHEV} = \begin{bmatrix} 0 & 1 \end{bmatrix}.$$
$$x = [\Delta P_{PHEV}], \quad u = [\Delta u_{PHEV}],$$
$$d = [\Delta n_{PHEV}], \quad y = [\Delta f].$$

MPC2: The state space of the control loop and the MPC calculation for the PV inverter can be expressed in (18)-(21).

$$\begin{bmatrix} \Delta \dot{P}_{PV} \\ \Delta \dot{f} \end{bmatrix} = \begin{bmatrix} \frac{-1}{T_{Inv}} & 0 \\ \frac{-1}{M} & \frac{-D}{M} \end{bmatrix} \begin{bmatrix} \Delta P_{PV} \\ \Delta f \end{bmatrix} + \begin{bmatrix} \frac{1}{T_{Inv}} \\ 0 \end{bmatrix} \Delta u_{PV} \tag{18}$$

$$[\Delta y] = \begin{bmatrix} 0 & 1 \end{bmatrix} \begin{bmatrix} \Delta P_{PV} \\ \Delta f \end{bmatrix} + [0]\, \Delta U_{PV}, \tag{19}$$

$$x(k+1) = A_{PV} \cdot x(k) + B_{PV} \cdot u(k) + G_{PV} \cdot d(k) \tag{20}$$

$$y(k) = C_{PV} \cdot x(k) + E_{PV} \cdot u(k) \tag{21}$$

where

$$A_{PV} = \begin{bmatrix} -1/T_{Inv} & 0 \\ -1/M & -D/M \end{bmatrix}, \quad B_{PV} = \begin{bmatrix} 1/T_{Inv} \\ 0 \end{bmatrix},$$
$$C_{PV} = \begin{bmatrix} 0 & 1 \end{bmatrix}, \quad E_{PV} = [0], \text{ and } G_{PV} = \begin{bmatrix} 0 & 0 \end{bmatrix}.$$
$$x = [\Delta P_{PV}], \quad u = [\Delta u_{PV}], \; y = [\Delta f].$$

REFERENCES

[1] S. Hashemi, J. Ostergaard, and G. Yang, "A scenario-based approach for energy storage capacity determination in LV grids with high PV penetration," *IEEE Trans. Smart Grid*, vol. 5, no. 3, pp. 1514–1522, May 2014.

[2] N. Sa-ngawong and I. Ngamroo, "Intelligent photovoltaic farms for robust frequency stabilization in multi-area interconnected power system based on PSO-based optimal Sugeno fuzzy logic control," *Renew. Energy*, vol. 74, pp. 555–567, Feb. 2015.

[3] M. Datta and T. Senjyu, "Fuzzy control of distributed PV inverters/energy storage systems/electric vehicles for frequency regulation in a large power system," *IEEE Trans. Smart Grid*, vol. 4, no. 1, pp. 479–488, Mar. 2013.

[4] S. Bahramirad, W. Reder, and A. Khodaei, "Reliability-constrained optimal sizing of energy storage system in a microgrid," *IEEE Trans. Smart Grid*, vol. 3, no. 4, pp. 2056–2062, Dec. 2012.

[5] H. Alharbi and K. Bhattacharya, "Stochastic optimal planning of battery energy storage systems for isolated microgrids," *IEEE Trans. Sustain. Energy*, vol. 9, no. 1, pp. 211–227, Jan. 2018.

[6] J. Pahasa and I. Ngamroo, "Coordinated control of wind turbine blade pitch angle and PHEVs using MPCs for load frequency control of microgrid," *IEEE Syst. J.*, vol. 10, no. 1, pp. 97–105, Mar. 2016.

[7] S. F. Aliabadi, S. A. Taher, and M. Shahidehpour, "Smart deregulated grid frequency control in presence of renewable energy resources by EVs charging control," *IEEE Trans. Smart Grid*, vol. 9, no. 2, pp. 1073–1085, Mar. 2018.

[8] K. D. Craemer, S. Vandael, B. Claessens, and G. Deconinck, "An event-driven dual coordination mechanism for demand side management of PHEVs," *IEEE Trans. Smart Grid*, vol. 5, no. 2, pp. 751–760, Mar. 2014.

[9] P. Goli and W. Shireen, "PV integrated smart charging of PHEVs based on DC link voltage sensing," *IEEE Trans. Smart Grid*, vol. 5, no. 3, pp. 1421–1428, May 2014.

[10] U. C. Chukwu and S. M. Mahajan, "V2G parking lot with PV rooftop for capacity enhancement of a distribution system," *IEEE Trans. Sustain. Energy*, vol. 5, no. 1, pp. 119–127, Jan. 2014.

[11] G. Carli and S. S. Williamson, "Technical considerations on power conversion for electric and plug-in hybrid electric vehicle battery charging in photovoltaic installations," *IEEE Trans. Power Electron.*, vol. 28, no. 12, pp. 5784–5792, Dec. 2013.

[12] J. M. Maciejowski, *Predictive Control: With Constraints*. Upper Saddle River, NJ, USA: Prentice-Hall, 2001.

[13] D. E. Seborg, T. F. Edgar, and D. A. Mellichamp, *Process Dynamics and Control*, 2nd ed. Hoboken, NJ, USA: Wiley, 2003.

[14] J. A. Rossiter, *Model-based Predictive Control: A Practical Approach*. Boca Raton, FL, USA: CRC Press, 2003.

[15] J. B. Rawlings and D. Q. Mayne, *Model Predictive Control: Theory and Design*. Madison, WI, USA: Nob Hill Publishing, 2009.

[16] A. Bemporad, M. Morari, and N. L. Ricker, "Model predictive control toolbox user's guide," Math Works, Natick, MA, USA, 2013.

[17] J. Pahasa and I. Ngamroo, "Simultaneous control of frequency fluctuation and battery SOC in a smart grid using LFC and EV controllers based on optimal MIMO-MPC," *J. Elect. Eng. Technol.*, vol. 12, no. 2, pp. 601–611, 2017.

[18] A. M. Ersdal, L. Imsland, and K. Uhlen, "Model predictive load-frequency control," *IEEE Trans. Power Syst.*, vol. 31, no. 1, pp. 777–785, Jan. 2016.

[19] M. Ma, H. Chen, X. Liu, and F. Allgöwer, "Distributed model predictive load frequency control of multi-area interconnected power system," *Electr. Power Energy Syst.*, vol. 62, pp. 289–298, Nov. 2014.

[20] T. H. Mohamed, H. Bevrani, A. Hassan, and T. Hiyama, "Decentralized model predictive based load frequency control in an interconnected power system," *Energy Convers. Manage.*, vol. 52, no. 2, pp. 1208–1214, 2011.

[21] P. M. Namara, R. R. Negenborn, B. D. Schutter, and G. Lightbody, "Optimal coordination of a multiple HVDC link system using centralized and distributed control," *IEEE Trans. Control Syst. Technol.*, vol. 21, no. 2, pp. 302–314, Mar. 2013.

[22] W. Qi, J. Liu, and P. D. Christofides, "Supervisory predictive control for long-term scheduling of an integrated wind/solar energy generation and water desalination system," *IEEE Trans. Control Syst. Technol.*, vol. 20, no. 2, pp. 504–512, Mar. 2012.

[23] A. Parisio, C. Wiezorek, T. Kyntäjä, J. Elo, K. Strunz, and K. H. Johansson, "Cooperative MPC-based energy management for networked microgrids," *IEEE Trans. Smart Grid*, vol. 8, no. 6, pp. 3066–3074, Nov. 2017.

[24] A. Ouammi, H. Dagdougui, L. Dessaint, and R. Sacile, "Coordinated model predictive-based power flows control in a cooperative network of smart microgrids," *IEEE Trans. Smart Grid*, vol. 6, no. 5, pp. 2233–2244, Sep. 2015.

[25] H. Farzin, M. Fotuhi-Firuzabad, and M. Moeini-Aghtaie, "Role of outage management strategy in reliability performance of multi-microgrid distribution systems," *IEEE Trans. Power Syst.*, vol. 33, no. 3, pp. 2359–2369, May 2018.

[26] J. Kennedy and R. Eberhart, "Particle swarm optimization," in *Proc. IEEE Int. Conf. Neural Netw.*, vol. 4, Nov./Dec. 1995, pp. 1942–1948.

[27] J. Cao, W. Du, H. Wang, and M. McCulloch, "Optimal sizing and control strategies for hybrid storage system as limited by grid frequency deviations," *IEEE Trans. Power Syst.*, vol. 33, no. 5, pp. 5486–5495, Feb. 2018.

[28] H. Li, D. Yang, W. Su, J. Lü, and X. Yu, "An overall distribution particle swarm optimization MPPT algorithm for photovoltaic system under partial shading," *IEEE Trans. Ind. Electron.*, vol. 66, no. 1, pp. 265–275, Jan. 2019.

[29] H. Shi, H. Wen, Y. Hu, and L. Jiang, "Reactive power minimization in bidirectional DC–DC converters using a unified-phasor-based particles swarm optimization," *Trans. Power Electron.*, vol. 33, no. 12, pp. 10990–11006, Dec. 2018.

[30] K. Sun, L. Zhang, Y. Xing, and J. M. Guerrero, "A distributed control strategy based on DC bus signaling for modular photovoltaic generation systems with battery energy storage," *IEEE Trans. Power Electron.*, vol. 26, no. 10, pp. 3032–3045, Oct. 2011.

[31] D. Maksimovic. ECEN2060 renewable sources and efficient electrical energy systems. University of Colorado Boulder. Accessed: Sep. 16, 2018. [Online]. Available: http://ecee.colorado.edu/ ecen2060/matlab.html

[32] S. Teleke, M. E. Baran, S. Bhattacharya, and A. Q. Huang, "Rule-based control of battery energy storage for dispatching intermittent renewable sources," *IEEE Trans. Sustain. Energy*, vol. 1, no. 3, pp. 117–124, Oct. 2010.

[33] J. Tan and Y. Zhang, "Coordinated control strategy of a battery energy storage system to support a wind power plant providing multi-timescale frequency ancillary services," *IEEE Trans. Sustain. Energy*, vol. 8, no. 3, pp. 1140–1153, Jul. 2017.

[34] F. Zhang *et al.*, "Improved cycle control and sizing scheme for wind energy storage system based on multiobjective optimization," *IEEE Trans. Sustain. Energy*, vol. 8, no. 3, pp. 966–977, Jul. 2017.

[35] Y. Cao, T. Wang, O. Kaiwartya, G. Min, N. Ahmad, and A. H. Abdullah, "An EV charging management system concerning drivers' trip duration and mobility uncertainty," *IEEE Trans. Syst., Man, Cyber. Syst.*, vol. 48, no. 4, pp. 596–607, Apr. 2018.

J. PAHASA received the B.Eng. degree from the King Mongkut's Institute of Technology Ladkrabang (KMITL), Bangkok, Thailand, in 1997, the M.Eng. degree from Chiang Mai University, Chiang Mai, Thailand, in 2007, and the D.Eng. degree from KMITL in 2011 all in electrical engineering.

She is currently an Assistant Professor with the School of Engineering, University of Phayao, Phayao, Thailand. Her current research interests include the applications of artificial intelligence in power system stability and control.

I. NGAMROO (SM'16) received the Ph.D. degree in electrical engineering from Osaka University, Osaka, Japan, in 2000.

He is currently a Professor with the Department of Electrical Engineering, Faculty of Engineering, King Mongkut's Institute of Technology Ladkrabang, Bangkok, Thailand. His research interests include power system stability, dynamic, and control.